J. Eur. Opt. Society-Rapid Publ. 2023, **19**, 47
© The Author(s), published by EDP Sciences, 2023
https://doi.org/10.1051/jeos/2023046
Available online at: https://jeos.edpsciences.org

Journal of the European Optical Society-Rapid Publications

RESEARCH ARTICLE OPEN ACCESS

The symmetric and antisymmetric phase modulation for the joint spectral amplitude of the biphotons in SPDC

Jinbao Wang[1,2] and Haibo Lin[2,*]

[1] College of Mechanical Engineering, Zhejiang University of Technology, Hangzhou 310014, China
[2] Institute of Mechanical & Electrical Technology, Taizhou Vocational & Technical College, Taizhou 318000, China

Received 6 November 2023 / Accepted 8 December 2023

Abstract. We analysis the generation of entangled biphotons by symmetric and antisymmetric phase modulation to obtain the corresponding joint spectral amplitude functions (JSAF) during the spontaneous parametric down-conversion (SPDC). With the help of Schmidt decomposition, the distribution probabilities of different modes are analyzed and the degree of entanglement is improved, which in turn leads to the effective regulation of entanglement, entropy, Schmidt coefficient and Schmidt number. Through simulations, we find that the antisymmetric phase modulation can slightly broaden the spectrum width, and the symmetric phase modulation distribution is more advantageous when the crystal is shorter.

Keywords: Biphotons, SPDC, Entanglement.

1 Introduction

Entanglements play a very important role in quantum mechanics for its rich properties which are specific characteristics for nonclassical physics. Especially for quantum swapping [1], quantum teleportation [2, 3], and quantum information [4], quantum dense coding [5], entanglement swapping [6, 7], and quantum cryptography [8, 9]. There are more ways to generate entanglement, the easiest of which is the entangled biphotons can be generated by spontaneous parametric down-conversion (SPDC) in nonlinear crystal. It shows the higher freedom degrees in spectral, space and polarization [10, 11]. In SPDC process, by varying factors to satisfy energy and momentum conservations, the entanglement can be higher, and the spectral entanglement shows the time is equivalent to the energy [11, 12]. These factors include the spectral entanglement by wave-vector direction, angular momentum and spatial [13–19], etc.

For the sake of simplicity, the entanglement can be controlled by polarization freedom. And the other appropriate freedoms, such as wavelength, frequency and time have been studied. In SPDC process, the pump photon can propagate the nonlinear crystal and interact with it, then split into two lower frequency photons named as signal light with frequency ω_s and idler one with frequency ω_i. The two photons are entangled with each other. The emission time is related with pump pulse duration time. It would eliminate the most distinguished information [6, 19]. However, a small part of the information cannot be eliminated for the different group velocity of the pump and signal field. The unvarnished information is caused by the strong correlation between the signal and idler photons. To make the entanglement be higher, many methods of adjust the multidimensional parametric such as the crystal length, materials and pump frequency bandwidth [19–23] are provided a better effect of the strong correlation.

For continuous parametric system, the analysis for the entanglement is mainly based on the discrete and infinite basis in the state function expression, which is need for the special mathematics [24, 25]. This analysis is a convenient theoretical expression for the quantity entanglement. And the biphotons quantum state shows the entangled freedom in Hilbert space. It means that when one of the quantum states of the biphotons can be formulated, the other one is also determined [11]. Here, to further explore the effects of symmetric and antisymmetric phase modulation on entanglement, we analysis the complex spectral function of the biphotons generated by SPDC. With the help of Schmidt decomposition, the continuous modes can be converted into specific discretized modes and the complex spectral functions can be compressed into the modes with more concise forms. The simplified modes have been analyzed and explored by the symmetric and antisymmetric phase modulation for the effective regulation of entanglement, entropy, Schmidt coefficient and Schmidt number with different length crystal.

* Corresponding author: linhaibo_tzvtc@163.com

This is an Open Access article distributed under the terms of the Creative Commons Attribution License (https://creativecommons.org/licenses/by/4.0), which permits unrestricted use, distribution, and reproduction in any medium, provided the original work is properly cited.

2 Theory for Schmidt decomposition

In this paper, we consider the polarization entanglement biphotons generated by type II SPDC. In generally, during SPDC, the pump pulse with higher frequency incidents the nonlinear crystal and interacts with it. It could emit into two photons named as signal and idler photons with lower frequency, the biphotons state vector for this process can be written as follows [26]:

$$\left|\Psi\right\rangle = \int J(\omega_s,\omega_i)a_s^{\dagger}(\omega_s)a_i^{\dagger}(\omega_i)|0\rangle_s|0\rangle_i \mathrm{d}\omega_s\mathrm{d}\omega_i, \quad (1)$$

where $a_\mu^{\dagger}(\omega_\mu)$ and $a_\mu(\omega_\mu)$ are the creation and annihilation operators of signal and idler lights ($\mu = s, i$) with frequency ω_s and ω_i respectively. $|0\rangle_\mu$ is the vacuum state. $J(\omega_s,\omega_i)$ is the original joint spectral amplitude function (JSAF) for the biphotons. It shows the correlation between the signal and idler photons which is caused by the interaction between the pump pulse and the nonlinear crystal. It directly determines the plenty properties such as spectral intensity, count rate and so on. If the JSAF $J(\omega_s,\omega_i)$ can be factorized into a product of the functions of the signal and idler photons, then there is no entanglement between them. Else, if the JSAF cannot be factorized into the inner product, then it can find that the biphotons is entangled. To analysis the JSAF $J(\omega_s,\omega_i)$, with the help Schmidt decomposition, it can be expressed as follows [26]

$$J(\omega_s,\omega_i) = \sum_n \sqrt{\lambda_n}u_n(\omega_s)v_n(\omega_i), \quad (2)$$

where $n = 1, 2,\ldots$ are the positive integer, λ_n are the eigenvalues which satisfy the normalization condition $\sum\lambda_n = 1$ [27]. $u_n(\omega_s)$ and $v_n(\omega_i)$ are the eigenfunctions for the following integral equations [26, 27]:

$$\int J(\omega_1,\omega_2)v_n^*(\omega_2)\mathrm{d}\omega_2 = \sqrt{\lambda_n}u_n(\omega_1), \quad (3)$$

$$\int u_n^*(\omega_1)J(\omega_1,\omega_2)\mathrm{d}\omega_1 = \sqrt{\lambda_n}v_n(\omega_2). \quad (4)$$

Meanwhile they can be written as:

$$\iint J(\omega,\omega_1)J^*(\omega',\omega_1)v_n(\omega')\mathrm{d}\omega_1\mathrm{d}\omega' = \int \rho_1(\omega,\omega')u_n(\omega')\mathrm{d}\omega'. \quad (5)$$

Also

$$\iint J(\omega_2,\omega)J^*(\omega_2,\omega')u_n(\omega')\mathrm{d}\omega_2\mathrm{d}\omega' = \int \rho_2(\omega,\omega')v_n(\omega')\mathrm{d}\omega', \quad (6)$$

where ρ_1 and ρ_2 are the kernels for the one photon spectral correlations, and they satisfy

$$\rho_1(\omega,\omega') = \int J(\omega,\omega_2)J^*(\omega',\omega_2)\mathrm{d}\omega_2, \quad (7)$$

$$\rho_2(\omega,\omega') = \int J(\omega_1,\omega)J^*(\omega_1,\omega')\mathrm{d}\omega_1. \quad (8)$$

u_n and v_n are conjugate Schmidt modes, and can be viewed as the eigenfunctions for these kernels:

$$\int \rho_1(\omega,\omega')u_n(\omega')\mathrm{d}\omega' = \lambda_n u_n(\omega), \quad (9)$$

$$\int \rho_2(\omega,\omega')v_n(\omega')\mathrm{d}\omega' = \lambda_n v_n(\omega). \quad (10)$$

The two orthogonal functions satisfy:

$$\int u_m^*(\omega_1)v_n(\omega_1)\mathrm{d}\omega_1 = \delta_{m,n}. \quad (11)$$

Equations (3) and (5) define the Schmidt modes in different ways. However, they are nearly equivalent to each other. The only difference is that the reduced density matrix cannot adjust the Schmidt modes phases. And to satisfy the relational equation of (5), it is necessary to include the corresponding arbitrary phase factor $\exp(i\theta_w)$. Phase modulation can be manipulated according to θ, where $\theta = 0$ and $\theta = \pi$ are the simplest cases, which denote the symmetric and antisymmetric ones. But when the Schmidt modes are defined by (3) with the addition of an arbitrary phase factor, the phase factors are determined, not a invariance anymore [27].

Here, we consider the type II SPDC, the ultrafast pump pulse incidents the nonlinear crystal and generates signal and idler photons. Because of the birefringence, the generated orthogonal polarization signal and idler photons are quite different. The different bandwidths can be viewed as a spectral information; it can be used to make the overlapping path as be distinguished. The frequency can help to definite which photon can arrival at the corresponding detector. Unless the JSAF for signal and idler photons is symmetry, signed as [28]

$$J(\omega_s,\omega_i) = J(\omega_i,\omega_s). \quad (12)$$

In symmetric structure, the signal and idler photons show the overlap of the determined band and narrow spectral, the joint amplitude function can be coherent superposition for each amplitude as follows [28]:

$$J_s(\omega_s,\omega_i,\theta) = J(\omega_s,\omega_i) + e^{i\theta}J(\omega_s,\omega_i), \quad (13)$$

where θ is the relative phase for the two amplitude functions. As $\theta = 0$, $J_s(\omega_s,\omega_i,0)$ is a symmetric structure. And $\theta = \pi$, $J_s(\omega_s,\omega_i,\pi)$ is antisymmetry.

When these photons are interference and $J(\omega_s,\omega_i)$ would be not symmetry as they are entangled. Because of the ω_s and ω_i auxiliary properties could show the photons path, it means that the state can be shown as:

$$|\Psi\rangle_s = \iint \mathrm{d}\omega_s\mathrm{d}\omega_i\left[J(\omega_s,\omega_i) + e^{i\theta}J(\omega_i,\omega_s)\right]|\omega_s\rangle|\omega_i\rangle. \quad (14)$$

It includes the overlap coherent for the original joint amplitude. However, this equation makes original joint amplitude spectral distinguished eliminate.

For the original joint amplitude function $J(\omega_s, \omega_i)$, it is caused by the interaction of the nonlinear crystal and the three mixed waves. So, it can be written as the product of pump envelop function $\chi(\omega_s, \omega_i)$ and the crystal phase matching function $\phi(\omega_s, \omega_i)$ [26, 29–31]

$$J(\omega_s, \omega_i) = \eta\chi(\omega_s, \omega_i)\phi(\omega_s, \omega_i), \tag{15}$$

where η is a normalized constant. And there are many cases of pump envelope functions, here, in this paper we mainly set it as Gaussian function with the function can be expressed as:

$$\chi(\omega_s, \omega_i) = \exp\left[-\frac{(\omega_s + \omega_i - 2\bar{\omega})^2}{\sigma^2}\right], \tag{16}$$

where σ is the pump light's bandwidth, $\bar{\omega}$ is the half of the central frequency for the pump pulse.

The phase matching function can be written as [32]

$$\phi(\omega_s, \omega_i) = \sin c\left(-\frac{\Delta kL}{2}\right)\exp\left(i\Delta kL\right). \tag{17}$$

Compare with the case in [26], we consider the phase factor $\exp(i\Delta kL)$ in the phase matching function and show its influence for the Schmidt modes. Here, Δk is the same expression as shown in [26].

$$\Delta k = k_p - k_s - k_i \simeq \sum_{\mu}\left(\omega_\mu - \bar{\omega}\right)\left(k'_p - k'_\mu\right), \tag{18}$$

Where $k = nc/\omega$ is the wave vector for the SPDC with frequency ω, n is the refractive index and c is the speed of in a vacuum. And the k'_μ represents the reciprocal of the group velocity for the generated photons (signal or idler) at frequency $\bar{\omega}$ and pump photon at frequency $2\bar{\omega}$.

3 Results and discussions

According to the conditions as shown above, we simulate the spectral power distributions as shown in Figure 1. We can find that the phase factor $\exp(i\Delta kL)$ in phase matching function could not essentially change the spectral power distribution. However, the increasing crystal length could decrease the JSAF's bandwidth. For all the cases, as the increasing of the crystal length, the response frequency bandwidth would be reduced (as see Figs. 1a and 1c, or 1b and 1d). The reason for this is that the product of the crystal length and the phase mismatch function constitutes the phase factor, and since the crystal length L is much less than one, the phase factor also tends to be more zero due to the smaller crystal length, which further extends the frequency response range. And the reverse is also true. By comparison, we can find that the original case is analogue to [26] and the peaks appear in the central with half of central frequency pump light, or signed $\bar{\omega}$ in this paper. Hence,

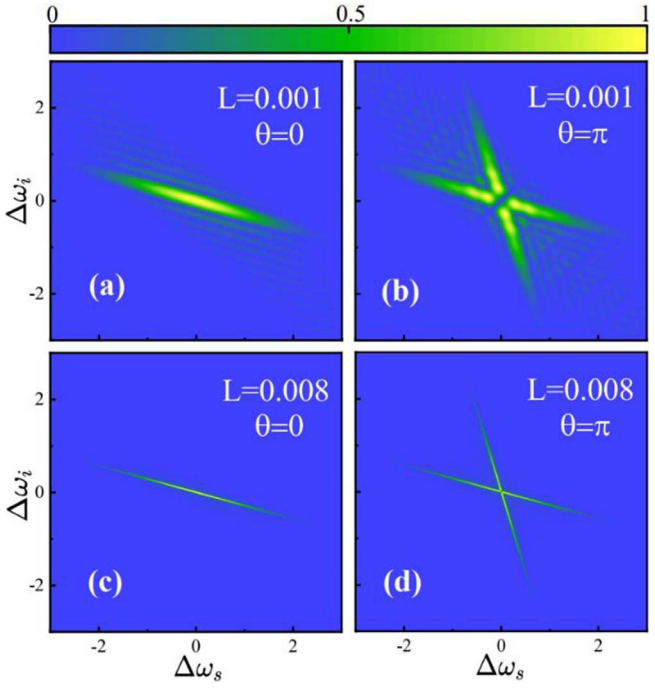

Figure 1. Spectral power distributions for nonlinear crystal with lengths (a), (b) $L = 0.001$ m and (c), (d) $L = 0.008$ m. The $\Delta\omega_{s,i}$ in the horizontal and vertical coordinates denote $\omega_{s,i} - \bar{\omega}$ and are in unit of σ, respectively. (a) and (c) are the symmetric structure with $\theta = 0$. (b) and (d) are the antisymmetric structure with $\theta = \pi$.

the first order phase factor of phase mismatching can essentially change the spectral intensity. For antisymmetric JSAF $J_s(\theta = \pi)$, its central frequency has no peaks, the spectral power distribution of JSAF changes from peaked to crossed, with the coarseness determined by the crystal length. The central spectral peak has been disappeared. It means that this case would be much more difficult to be factorized. However, the spectral intensity is symmetric with central point, and would be more complicated to original one, which is analogue to [26]. In the antisymmetric case, the crossed spectral power distribution of JSAF indicates that maybe there are many degenerated states in this case. According to Figures 1b and 1d, the shorter the crystal length, the wider the frequency domain width of the degenerated states. This is mainly due to the fact that the product of the crystal length $L(L < 1)$ and the phase mismatch function Δk avoids drastic oscillations in the phase factor and extends the frequency width. Meanwhile, when the crystal length is $L = 0.001$ m, it can be found that there are fluctuations with small amplitude around the main peak of the spectral power distribution for JSAF. This is mainly caused by the interaction between the phase mismatch function Δk with the nonlinear crystal.

According to Schmidt decomposition, we can obtain the modes distribution in antisymmetric JSAF($\theta = \pi$). Because of eigenvalue is focused on the front ones, we choose the modes with $n = 1, 2$. Figure 2 represents the Schmidt modes when the symmetric and antisymmetric JSAFs are

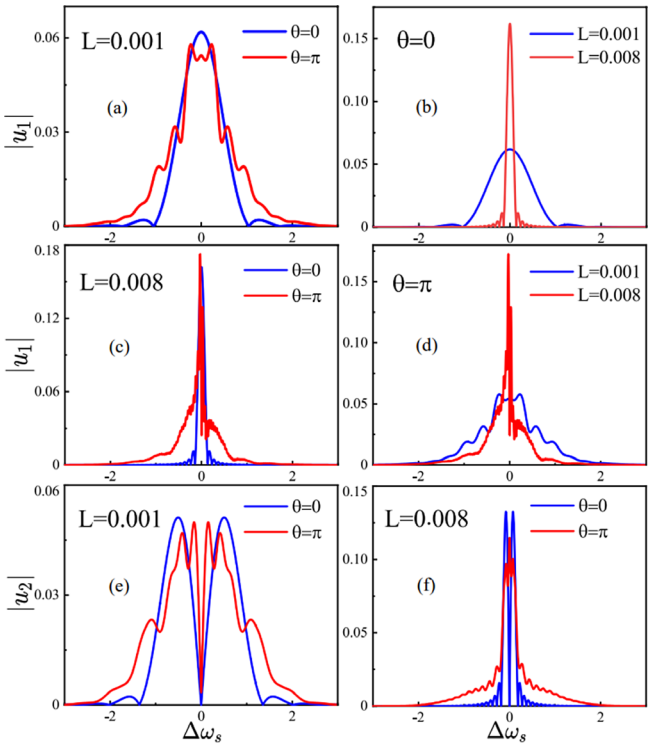

Figure 2. The distribution of the Schmidt modes at the main (taking $n = 1, 2$) obtained by the Schmidt decomposition. It is also the distribution of the Schmidt states of the frequency-domain content in Figure 1.

decomposed, and only the modes with $n = 1, 2$ are shown here. Through Figure 2, it can be found that for the same θ, the increase of crystal length compresses the width of the frequency domain, especially when $\theta = 0$, the effect is most obvious (see Fig. 2b). And $\theta = \pi$, not only breaks the peaks in the original JSAF (see Fig. 2a, which also coincides with the conclusion in Fig. 1), but also increases the frequency domain width to some extent, see Figures 2a–2d. Also, as the crystal length increases, $\theta = \pi$ tends to break the symmetry of the Schmidt mode. And as the number of modes n increases, the number of peaks in the corresponding modes also increases, which is very obvious when the crystal length is short. However, as the crystal length increases, the symmetry and the law of the number of wave peaks are somewhat broken by $\theta = \pi$.

For the eigenvalues λ_n and their entanglement entropy, the phase factor $\exp(i\Delta kL)$ in phase matching function cannot essentially change the result. We can obtain the 50 eigenvalues after decomposition the original and antisymmetric JSAF as shown in Figure 3. In this figure, it can be found that the main eigenvalue ($n < 6$) has located 95% of all eigenvalues. Of course, the entanglement entropy with $n < 6$ has located 90% of all sum. Hence, the first 6 modes are the main base. It means the vector has been curtailed low dimensional space. It can be found through this figure that the shorter the crystal length is, the larger proportion of the first few eigenvalues among all eigenvalues is. For example, in the symmetric case ($\theta = 0$) with the crystal length $L = 0.001$ m, $\lambda_1 \approx 0.6$, and $\lambda_2 \approx 0.3$, these two eigenvalues occupy the majority of the proportion, which means that these two modes appear in the highest possibility. It is favorable for the selection and simplification of the Schmidt modes. As for the antisymmetric case ($\theta = \pi$), many pairs with the same value of eigenvalues appear, which implies the existence of the degenerated states, consistent with the prediction in Figure 1. As the crystal length increases, the difference between the first few eigenvalues become smaller and smaller. However, when $L = 0.008$ m, there are still degenerated states in the antisymmetric state, since their $\lambda_1 = \lambda_2$. Overall, we are more concerned with the case of crystals $L = 0.001$ m, when $\theta = \pi$, the largest eigenvalue $\lambda_n \approx 0.37$, with degenerated pairs in antisymmetric with $n < 6$, much lower, nearly half of the λ_1 in original case. It means the modes have been split into degenerate pairs of modes which owns the same possibility.

Here, the entropy can be obtained based the eigenvalue according to the equation as follows [26]:

$$S = -\sum_{k=1}^{n} \lambda_k \log_2 \lambda_k. \tag{19}$$

As the analysis based on Figure 3a, we can find that the entangled entropy turns to converge as $n \to \infty$ for both in original and antisymmetric JSAF. This is consistent with the conclusion that the eigenvalues converge to 0 as $n \to \infty$. Moreover, when $L = 0.001$ m and $\theta = 0$, the entropy already reaches a maximum value of about 1.6 at $n = 6$. It also implies that the $n \leq 6$ modes with play significant roles of all modes. It agrees with the distribution of the eigenvalues in Figure 3a. Besides, the increase of mode distributions in antisymmetric makes the entangled entropy be larger, from about 1.6 in original case to about 2. This is mainly due to the fact that in the antisymmetric case, there are degenerated states and it is not possible to highlight a single state. Essentially, the entangled entropy is deeply dependent on the main eigenvalues. The value of entropy gradually increases as the length of the crystal increases. And it is mainly determined by the first few values of n. The shorter the crystal length, the slower its entropy increases, corresponding to a greater proportion of the first few eigenvalues contributed. With the increase of n, the values of entropy tend to converge and stabilize gradually. As the crystal length increases, the entropy distributions for the symmetric and antisymmetric cases are also not particularly noticeable when the crystal length $L = 0.008$ m, since the role of the front mode cannot be highlighted (as shown in Fig. 3b).

For each eigenvalue and Schmidt mode, the new Schmidt coefficient C_n can be introduced to indicate the distributions for different modes. It can be shown as [32]:

$$C_n = \frac{\left[\sinh\left(G\sqrt{\lambda_n}\right)\right]^2}{\sum_n \left[\sinh\left(G\sqrt{\lambda_n}\right)\right]^2}, \tag{20}$$

where G is the parametric gain and set $G = 1$ in Figure 4a. It shows that the shorter of the crystal, the less effective number of the modes, which could help to concentrate on these modes. For example, when $L = 0.001$ m and $\theta = 0$, the coefficients vary very sharp for $n \leq 6$. It implies

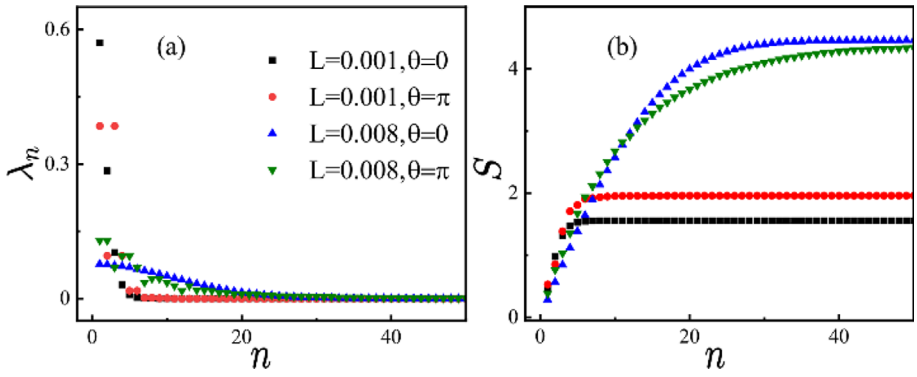

Figure 3. (a) Eigenvalues λ_n and (b) the entropy function S with n for the symmetric and antisymmetric JSAF for two lengths of the nonlinear crystal. The legend in plot (b) is the same with the one shown in plot (a).

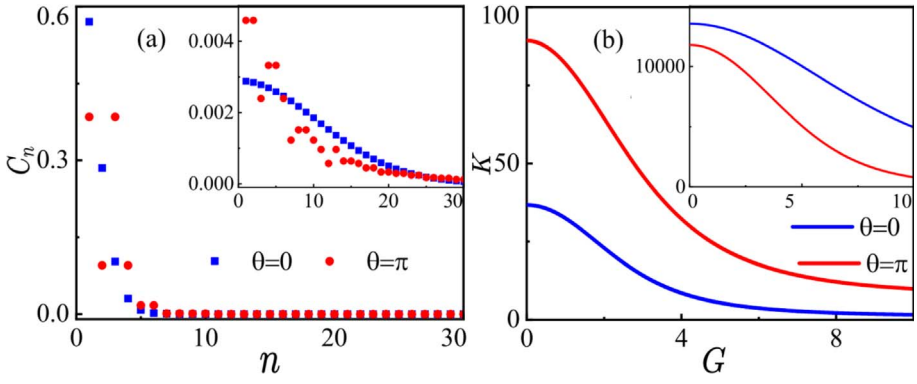

Figure 4. (a) Coefficient C_n of the Schmidt modes and (b) K for symmetric and antisymmetric JSAF of SPDC with the crystal length $L = 0.001$ m (main plots) and $L = 0.008$ m (inset plots).

that the corresponding Schmidt modes occupy with larger probability. While $\theta = \pi$, many pairs with the same coefficients appear for the reason of degenerated states. It is entirely consistent with the findings in Figure 3.

Meanwhile, these effective number can be defined by the Schmidt number which can be express as following [32–35]:

$$K = \frac{1}{\sum_n C_n}. \tag{21}$$

The Schmidt number versus the parametric gain G is shown in Figure 4b, these plots show that only the fronts Schmidt modes could contribute to the SPDC and could define all properties of SPDC as the high parametric gain. Especially for the symmetric JSAF with short length of the nonlinear crystal. Therefore, for crystals with short length crystal with high gain, symmetric JSAF can be decomposed into the modes with a higher probability, which is helpful to be studied and explored in lower dimensions.

4 Conclusion

We analysis the symmetric and antisymmetric phase modulation of JSAF for the entangled biphotons generated by SPDC through Schmidt decomposition. The distribution probabilities of different modes are analyzed and the degree of entanglement is improved, which in turn leads to the effective regulation of entanglement, entropy, Schmidt coefficient and Schmidt number. Through simulations, we find that the phase factor $\exp(i\Delta kL)$ in phase matching function could not essentially change the spectral power distribution. And the antisymmetric phase modulation can slightly broaden the spectrum width, and the symmetric phase modulation distribution is more advantageous when the crystal is shorter. We hope that our work will be help to improve the degree of entanglement and effectively modulate of Schmidt number for the ultrashort pulses.

Competing interests

The authors declare that they have no competing interests.

Authors' contributions

JW proposed the original idea, gave advices and wrote the manuscript. HL implemented the work. The progress is a result of common contributions and discussions of JW and HL. Both authors read and approved the final manuscript.

Acknowledgments. This work was supported by General scientific research project of Zhejiang Provincial Department of Education (Grant No. Y202250327), Taizhou Science and Technology Project (Grant No. 22gyb17), and Taizhou High-level Talent Special Support Program (2019, 2020).

References

1 Pan J.W., Bouwmeester D., Weinfurter H., Zeilinger A. (1998) Experimental entanglement swapping: entangling photons that never interacted, *Phys. Rev. Lett.* **80**, 18, 3891.
2 Bouwmeester D., Pan J.W., Mattle K., Eibl M., Weinfurter H., Zeilinger A. (1997) Experimental quantum teleportation, *Nature* **390**, 575.
3 Bouwmeester D., Mattle K., Pan J.W., Weinfurter H., Zeilinger A., Zukowski M. (1998) Experimental quantum teleportation of arbitrary quantum states, *Appl. Phys. B: Lasers Opt.* **67**, 749.
4 Bennett C.H., Shor P.W. (1998) Quantum information theory, *IEEE Trans. Inf. Theory* **44**, 2724.
5 Mattle K., Weinfurter H., Kwiat P.G., Zeilinger A. (1996) Dense coding in experimental quantum communication, *Phys. Rev. Lett.* **76**, 4656.
6 Zukowski M., Zeilinger A., Horne M.A., Eckert A.K. (1993) "Event-ready-detectors" Bell experiment via entanglement swapping, *Phys. Rev. Lett.* **71**, 4287.
7 Pan J.W., Bouwmeester D., Weinfurter H., Zeilinger A. (1998) Experimental entanglement swapping: entangling photons that never interacted, *Phys. Rev. Lett.* **80**, 3891.
8 Eckert A.K. (1991) Quantum cryptography based on Bell's theorem, *Phys. Rev. Lett.* **67**, 661.
9 Townsend P.D., Rarity J.G., Tapster P.R. (1993) Single photon interference in 10 km long optical fibre interferometer, *Electron. Lett.* **29**, 634.
10 Klyshko D.N. (1980) *Photons and Nonlinear Optics*, Nauka, Moscow.
11 Saleh M.F., Saleh B.E.A., Teich M.C. (2009) Modal, spectral, and polarization entanglement in guided-wave parametric down-conversion, *Phys. Rev. A.* **79**, 053842.
12 Saleh B.E.A., Abouraddy A.F., Sergienko A.V., Teich M.C. (2000) Duality between partial coherence and partial entanglement, *Phys. Rev. A* **62**, 043816.
13 Mair A., Vaziri A., Weihs G., Zeilinger A. (2001) Entanglement of the orbital angular momentum states of photons, *Nature (London)* **412**, 313.
14 Joobeur A., Saleh B.E.A., Teich M.C. (1994) Spatiotemporal coherence properties of entangled light beams generated by parametric down-conversion, *Phys. Rev. A* **50**, 3349.
15 Joobeur A., Saleh B.E.A., Larchuk T.S., Teich M.C. (1996) Coherence properties of entangled light beams generated by parametric down-conversion: theory and experiment, *Phys. Rev. A* **53**, 4360.
16 Abouraddy F., Yarnall T., Saleh B.E.A., Teich M.C. (2007) Violation of Bell's inequality with continuous spatial variables, *Phys. Rev. A* **75**, 052114.
17 Yarnall T., Abouraddy A.F., Saleh B.E.A., Teich M.C. (2007) Experimental violation of Bell's inequality in spatial-parity space, *Phys. Rev. Lett.* **99**, 170408.
18 Menzel R., Puhlmann D., Heuer A. (2017) Complementarity in single photon interference – the role of the mode function and vacuum fields, *J. Eur. Opt. Soc. Rapid Publ.* **13**, 8.
19 Grice W.P., U'Ren A.B., Walmsley I.A. (2001) Eliminating frequency and space-time correlations in multiphoton states, *Phys. Rev. A* **64**, 063815.
20 Short A.J., Popescu S., Gisin N. (2006) Entanglement swapping for generalized nonlocal correlations, *Phys. Rev. A* **73**, 012101.
21 Fanchini F.F., Cornelio M.F., de Oliveira M.C., Caldeira A.O. (2011) Conservation law for distributed entanglement of formation and quantum discord, *Phys. Rev. A* **84**, 012313.
22 Kogias I., Lee A.R., Ragy S., Adesso G. (2015) Quantification of Gaussian quantum steering, *Phys. Rev. Lett.* **114**, 060403.
23 Boudreault C., Berthiere C., Krempa W.W. (2022) Entanglement and separability in continuum Rokhsar-Kivelson states, *Phys. Rev. Res.* **4**, 033251.
24 Parker S., Bose S., Plenio M.B. (2000) Entanglement quantification and purification in continuous-variable systems, *Phys. Rev. A.* **61**, 032305.
25 Leohardt U. (1997) *Measuring the Quantum State of Light*, Cambridge University Press, Combridge, England.
26 Law C.K., Walmsley I.A., Eberly J.H. (2000) Continuous frequency entanglement: effective finite Hilbert space and entropy control, *Phys. Rev. Lett.* **84**, 5304.
27 Fedorov M.V., Miklin N.I. (2014) Schmidt modes and entanglement, *Contemp. Phys.* **55**, 2, 94–109.
28 Branning W.P., Grice R.Erdmann, Walmsley I.A. (1999) Engineering the indistinguishability and entanglement of two photons, *Phys. Rev. Lett.* **83**, 995.
29 Ou Z.Y. (1997) Parametric down-conversion with coherent pulse pumping and quantum interference between independent fields, *Quantum Semiclass. Opt.* **9**, 599.
30 Keller T.E., Rubin M.H. (1997) Theory of two-photon entanglement for spontaneous parametric down-conversion driven by a narrow pump pulse, *Phys. Rev. A* **56**, 1534.
31 Grice W.P., Walmsley I.A. (1997) Spectral information and distinguishability in type-II down-conversion with a broadband pump, *Phys. Rev. A* **56**, 1627.
32 Sharapova P.R., Tikhonova O.V., Lemieux S., Boyd R.W., Chekhova M.V. (2018) Bright squeezed vacuum in a nonlinear interferometer: frequency and temporal Schmidt-mode description, *Phys. Rev. A.* **97**, 053827.
33 Allevi A., Jedrkiewicz O., Brambilla E., Gatti A., Perina J. Jr., Haderka O., Bondani M. (2014) Coherence properties of high-gain twin beams, *Phys. Rev. A* **90**, 063812.
34 Dyakonov I.V., Sharapova P.R., Iskhakov TSh, Leuchs G. (2015) Direct Schmidt number measurement of high-gain parametric down conversion, *Laser Phys. Lett.* **12**, 065202.
35 Guo X., Liu N., Li X., Ou Z.Y. (2016) Complete temporal mode analysis in pulse-pumped fiber-optical parametric amplifier for continuous variable entanglement generation, *Opt. Express* **23**, 29369.
36 Liñares J., Carral G.M., Prieto-Blanco X., Balado D. (2021) Autocompensating measurement-device-independent quantum cryptography in space division multiplexing optical fibers, *J. Eur. Opt. Soc. Rapid Publ.* **17**, 19.